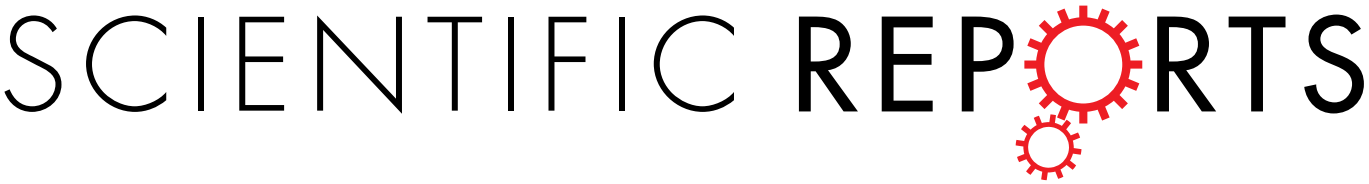

OPEN

A magnetoelectric flux gate: new approach for weak *DC* magnetic field detection

Received: 8 June 2017
Accepted: 24 July 2017
Published online: 17 August 2017

Zhaoqiang Chu[1], Huaduo Shi[1], Mohammad Javad PourhosseiniAsl[1], Jingen Wu[1], Weiliang Shi[1], Xiangyu Gao[1], Xiaoting Yuan[1] & Shuxiang Dong[1,2]

The *magnetic flux gate* sensors based on Faraday's Law of Induction are widely used for *DC* or extremely low frequency magnetic field detection. Recently, as the fast development of multiferroics and magnetoelectric (ME) composite materials, a new technology based on ME coupling effect is emerging for potential devices application. Here, we report a *magnetoelectric flux gate* sensor (MEFGS) for weak *DC* magnetic field detection for the first time, which works on a similar *magnetic flux gate* principle, but based on ME coupling effect. The proposed MEFGS has a shuttle-shaped configuration made of amorphous FeBSi alloy (Metglas) serving as both magnetic and magnetostrictive cores for producing a closed-loop high-frequency magnetic flux and also a longitudinal vibration, and one pair of embedded piezoelectric PMN-PT fibers ([011]-oriented $Pb(Mg,Nb)O_3$-$PbTiO_3$ single crystal) serving as *ME flux gate* in a differential mode for detecting magnetic anomaly. In this way, the relative change in output signal of the MEFGS under an applied *DC* magnetic anomaly of 1 nT was greatly enhanced by a factor of 4 to 5 in comparison with the previous reports. The proposed *ME flux gate* shows a great potential for magnetic anomaly detections, such as magnetic navigation, magnetic based medical diagnosis, etc.

Multiferroic magnetoelctric (ME) materials have been attracting considerable interest due to the potential application, particularly in terms of magnetic field sensors, microelectromechanical system, tunable microwave devices, tunable bandpass/bandstop filters, tunable phase shifters and spintronics, etc, since the last two decades[1–6]. It has been investigated and proved that multi-phase ME composites are able to exhibit much better ME coupling effect than single phase ME materials at room temperature[7–9]. In recent years, a variety of bulk ME composites with different phase connectivity, i.e., (0-3), (1-3), (2-2), (2-1), or (1-1), have been paid extensive attention, and tremendous progress has been achieved[10–19]. To date, one-dimensional (1-1) connectivity ME composites consisting of a [011]-oriented $Pb(Mg,Nb)O_3$-$PbTiO_3$ (PMN-PT) single crystal fiber laminated with laser-treated amorphous FeBSi alloy (Metglas) and operating in *L-T* mode (longitudinally magnetized and transversely poled) achieved the highest resonance ME coefficient of $\sim 7\,kV\,cm^{-1}\,Oe^{-1}$ in the case of bulk composites[19]. In addition, ME thin film cantilever type sensors made of AlN and FeCoSiB could possess a high resonance ME coupling coefficient of $5\,kV\,cm^{-1}\,Oe^{-1}$ in the air, and even $20\,kV\,cm^{-1}\,Oe^{-1}$ in vacuum[20,21].

In spite of the significant advances, it is always and will remain an open challenge in sensing weak *DC* and extremely low frequency *AC* (ranging from 10 mHz to 10 Hz) magnetic fields due to the large $1/f$ noise[22–25]. In this respect, magnetic sensors based on *flux gate* principle, superconducting quantum interference effect (SQUIDs), tunneling magnetoresistance(TMR), anisotropic magnetoresistance (AMR), giant magnetoresistance (GMR), giant magnetoimpedance (GMI), and nonlinear magnetoelectric effect have intrigued dramatic research interests[26–30]. However, the applications of magnetic sensors are subjected to many limitations. For example, SQUIDs-based devices requires extremely low operation temperature, which leads to high manufacture and maintenance cost[26]. The need for an external magnetic bias for TMR, GMR and GMI sensors to optimize the sensitivity inevitably increases the volume and power consumption of a detection system[27–29]. In addition, the resistance variation in terms of AMR or GMR sensors is quite low in responding to weak magnetic field[27,29,30]. Furthermore, the frequency conversion technology based on nonlinear ME effect fails to work when it comes to the measurement of *DC* magnetic field[22,23]. It is well known that *flux gate* sensors are able to detect small *DC* magnetic fields, typically, from 0.5 nT to 100 μT, and now they have been widely used in the market[31–36]. Unfortunately,

[1]Department of Materials Science and Engineering, College of Engineering, Peking University, Beijing, 100871, China. [2]Beijing Key Laboratory for Magnetoeletric Materials and Devices, Beijing, 100871, China. Correspondence and requests for materials should be addressed to S.D. (email: sxdong@pku.edu.cn)

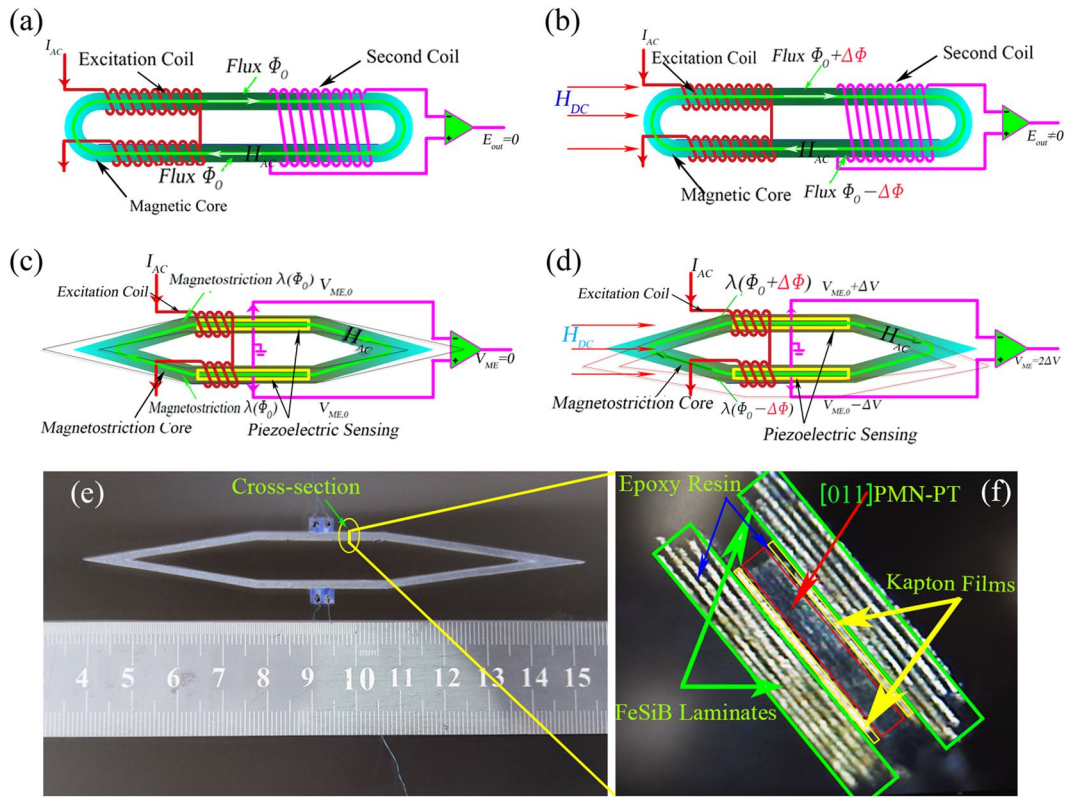

Figure 1. Schematic representation of the conventional flux gate senor and our proposed magnetoelectric flux gate sensor. The structure of (**a**), (**b**) a race-track *flux gate* sensor and (**c**), (**d**) our proposed *Magnetoelectric (ME) flux gate* sensor; (**a**), (**c**) in the absence of *DC* magnetic field (H_{DC}); (**b**), (**d**) in the presence of *DC* magnetic field (H_{DC}); (**e**) A photograph of the actual *ME flux gate*; (**f**) A cross-sectional optical image of the ME composites.

their power consumption tends to be rather high since the requirement to saturate the magnetic core materials periodically[37].

In this paper, we report a shuttle-shaped, non-biased *magnetoelectric flux gate* sensor (MEFGS) enlightened by the working mechanism and configuration of the *magnetic flux gate* sensors[31,35]. We have studied its working mechanism in comparison with *flux gate* sensors and characterized the ME performance as well. In addition, we also investigate its absolute *DC* magnetic field sensitivity in comparison with those based on the conventional magnetic detection technologies. We will see the relative change in output signal of the MEFGS under an applied *DC* magnetic anomaly of 1 nT was greatly enhanced by a factor of 4 to 5 in comparison with the previous reports.

Results

Structure design and working principle. Conventional *flux gate* magnetic sensors are based on Faraday's Law of Induction for magnetic anomaly detection. Figure 1(a) and (b) show the structure and working principle of a racetrack *magnetic flux gate* sensor. As shown in Fig. 1(a), the *flux gate* sensor is composed of a racetrack type magnetic core surrounded by an excitation (first) coil and a detection (second) coil. The first coil is used for exciting an *AC* magnetic field H_{AC}, which produces a closed-loop flux Φ_0 in the racetrack magnetic core and saturates the magnetic core materials periodically. The second coil is used for detecting magnetic anomaly (H_{DC})[35]. In the case of (H_{DC}) = 0, the output of the *magnetic flux gate* sensor could be absent in theory, since the net magnetic flux Φ ($=\Phi_0-\Phi_0$) passing through the second coil is zero, as shown in Fig. 1(a). However, we could expect an effective output signal $E_{out} = -2d\Delta\Phi/dt$, from the second coil in the presence of *DC* magnetic field H_{DC}, because there is a net magnetic flux Φ ($=2\Delta\Phi$) passing through the second coil, see Fig. 1(b).

In a similar way as described in Fig. 1(a) and (b), a *magnetoelectric flux gate* sensor (MEFGS) is designed into a shuttle-shaped structure (instead of a racetrack structure) with an excitation coil and one pair of piezoelectric sensing elements (instead of second coil), as shown in Fig. 1(c) and (d). When a constant *AC* current I_{AC} passes through the excitation coil, a closed-loop high-frequency magnetic field H_{AC} and flux Φ_0 can be excited in the magnetic core, which induces a symmetric elongating and shrinking of two halves due to the magnetostrictive effect. Therefore, a longitudinal vibration mode of the shuttle-shaped structure is produced, and correspondingly, the difference output ME signal from ME gate will be zero due to symmetric vibration in the absence of an applied *DC* magnetic field, as shown in Fig. 1(c) with dash line.

However, once a *DC* magnetic anomaly appears, the magnetic field increases in one half, and while it decreases in another half, which then causes unsymmetrical elongating and shrinking in two halves of the structure. As a result, the initial longitudinal vibration mode of the shuttle-shaped structure tends to be a longitudinal-bending

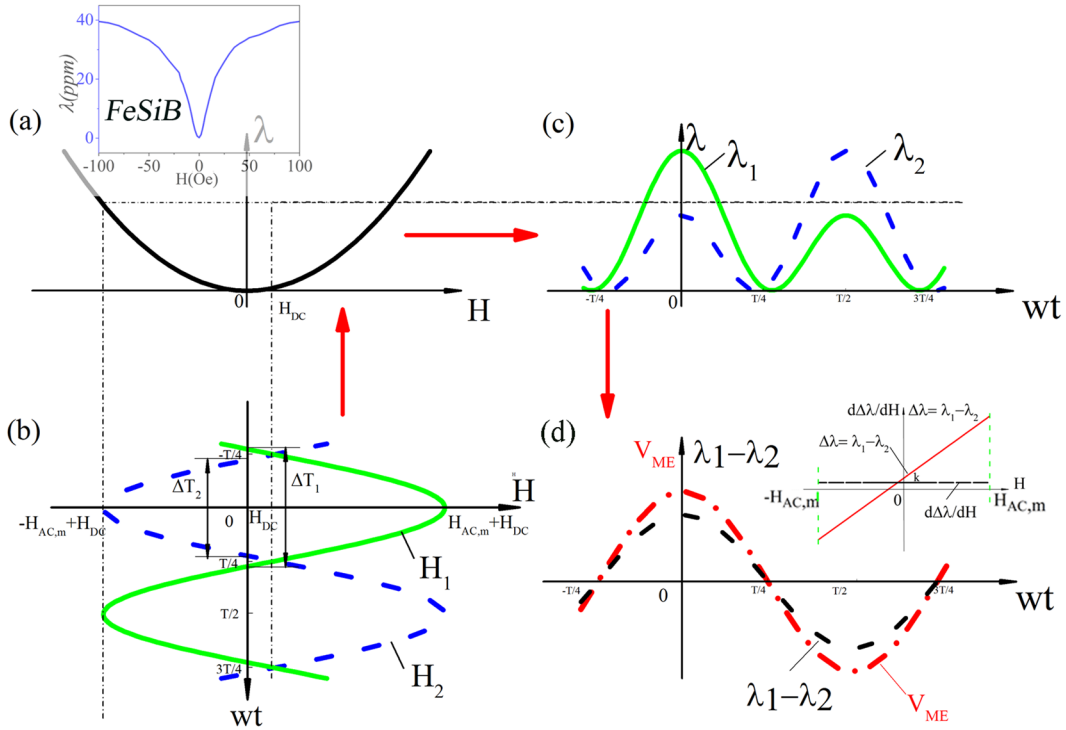

Figure 2. The working principle of our proposed magnetoelectric flux gate sensor. (**a**) The magnetostrictive curve of magnetic core; (**b**) the magnetic field in top half: $(H_{AC}+H_{DC})$, while in bottom half: $(-H_{AC}+H_{DC})$; (**c**) The double-frequency magnetostrictions of λ_1 and λ_2 in time domain for two half magnetic cores (1# and 2#); (**d**) The magnetostrictive difference $\Delta\lambda$ and the ME signal difference ΔV_{ME} of two halves in time domain in same-frequency first harmonic signal form; the inset is $\Delta\lambda$ as a function of H_{DC} and its derivative with respect to H_{DC}.

one due to the effect of magnetic anomaly H_{DC}, as shown in Fig. 1(d) with dash line. In this case, the differential signal output from *ME flux gate* will be non-zero.

With respect to a *flux gate* sensor, the induced E_{out} from the second coil under H_{DC} can be found as ref. 34

$$E_{out} = -N_s A_s \frac{d(\Delta B)}{dt} = -2N_s A_s \frac{d^2 B}{dHdt} H_{DC}, \tag{1}$$

in which E_{out} is proportional to H_{DC}. Note that E_{out} is a *second harmonic signal* relative to H_{AC}. When it comes to the proposed *ME flux gate* sensor, the working mechanism, which is similar to that of *flux gate* sensor, is illustrated in Fig. 2. The magnetostrictive curve is assumed to be a quadratic function of H ($\lambda = kH^2$, where k is a parameter related to the magnetostrictive performance of magnetic material), as shown in Fig. 2(a). Here assuming the exciting magnetic field $H_{AC} = H_m\cos(\omega t)$ is small. In the case without an external magnetic field H_{DC}, H_{AC} in top half of the shuttle-shaped magnetostrictive core is equal to that in bottom half in amplitude, but they are in reverse phase. H_{AC} then excites two symmetric but frequency-doubling magnetostrictions $\lambda_1(H_{AC})$ and $\lambda_2(-H_{AC})$ in two halves of the shuttle-shape magnetic core. Therefore, the induced two ME signals from one pair of piezoelectric sensing elements will be completely identical, resulting a zero output signal from *ME flux gate* due to its differential mode. However, when an additional external magnetic field H_{DC} appears, see Fig. 1(d), the magnetic field in top half will become $(H_{AC}+H_{DC})$, while in bottom half it becomes $(-H_{AC}+H_{DC})$, as they are shown in a time domain in Fig. 2(b). Therefore, the magnetostrictions $\lambda_1(H_{AC}+H_{DC})$ produced in top half and $\lambda_2(-H_{AC}+H_{DC})$ in bottom half will become asymmetric, as they are presented in time domain in Fig. 2(c). The asymmetric magnetostrictions in two halves further induce asymmetric two ME signals due to ME coupling effect, and their differential output ΔV_{ME} from *ME flux gate* is non-zero that is directly proportional to the external magnetic field H_{DC}, see Fig. 2(d).

Now we try to find the relationship between ΔV_{ME} and H_{DC}. Assuming a *DC* magnetic filed H_{DC} appearing along longitudinal axis direction, as shown in Fig. 1(d), and further assuming the applied H_{DC} is small, the magnetostrictive difference $\Delta\lambda$ between two halves is

$$\Delta\lambda = \lambda_1 - \lambda_2 \approx 2\frac{d\lambda}{dH} H_{DC}. \tag{2}$$

It is well known the output ME voltage V_{ME} can be written as ref. 23

$$V_{ME} = \alpha_{ME} \cdot t_p \cdot H_{AC} = \frac{\partial E}{\partial \sigma} \cdot \frac{\partial \sigma}{\partial \lambda} \cdot \frac{\partial \lambda}{\partial H} \cdot t_p \cdot H_{AC}, \tag{3}$$

where α_{ME} is the ME coupling coefficient, σ is the mechanical stress, and t_p is the thickness of the piezoelectric phase. Considering that the *ME flux gate* sensor working in a differential mode, the output differential ME voltage ΔV_{ME} can be expressed as follow[23]:

$$\Delta V_{ME} = t_p \frac{\partial E}{\partial \sigma} \frac{\partial \sigma}{\partial \lambda} \frac{\partial (\Delta \lambda)}{\partial H} H_{AC} = -t_p \frac{g_{32,p}}{s_{33}^*} 2kH_{AC}H_{DC}, \tag{4}$$

where $g_{32,p} = -\frac{\partial E_3}{\partial \sigma_2}$ is the transverse piezoelectric voltage constant of the [011]-oriented PMN-PT; $s_{33}^* = 1/(\frac{\partial \sigma_3}{\partial \lambda_3})$ is the equivalent elastic compliance of the ME composite; $k = \frac{\partial^2 \lambda}{\partial H^2}$ is a constant associated with material properties. The output differential ME voltage ΔV_{ME} in time domain is *first harmonic signal*, as shown in Fig. 2(d). Note that the ME voltage ΔV_{ME} is proportional to both H_{DC} and H_{AC}.

It should be pointed that if the *DC* magnetic field is completely absent, the magnetostrictions of the two halves of the shuttle-shape magnetic core exhibit *frequency-doubling effect*. Frequency doubling and harmonic distortion behaviors in laminated ME composite have been previously studied theoretically and experimentally[38–42]. *Dmitrii et al*. reported a *DC* magnetic field detection with a responsibility of 2.5 V/mT based on the nonlinear magnetoelectric effect of a well-known sandwiched ME structure[42]. In the shuttle-shaped *ME flux gate* sensor, from the Equation 4, the output voltage ΔV_{ME} should be zero in theory when there is no applied field H_{DC}. Once a H_{DC} appears, ΔV_{ME}, which is proportional to H_{DC}, is induced, and it exhibits the same-frequency harmonic signal as that of H_{AC}, i.e., the frequency-doubling phenomenon will disappear. Clearly, "frequency-doubling" to "same-frequency" phenomenon may be an important criterion to indicate H_{DC} appearing. While differing from it, the "same-frequency" to "*frequency-doubling*" phenomenon may be an important criterion to indicate H_{DC} appearing for a *flux gate* sensor. Therefore, the proposed *ME flux gate* sensor offers a new approach for *DC* magnetic field detection, and it will be expected to possess the equal or even better performance for sensing extremely weak *DC* magnetic field in comparison with *magnetic flux gate* sensor, but it has much lower power consumption and also much smaller sizes.

Materials fabrication and mechanism confirmation. We fabricated a *magnetoelectric flux gate* sensor. The magnetic core of MEFGS is made of laser-treated amorphous FeBSi alloy (Metglas) which has a high permeability and also piezomagnetic effect. The methods concerning the laser treatment and the sensor fabrication have been reported by *Chu et al*.[19]. One pair of [011]-oriented PMN-PT single crystal fibers (as labeled as 1# and 2#) were embedded in the magnetic core. Figure 1(e) shows the prototype of our proposed *ME flux gate* sensor and the cross-sectional optical microscopy image of the ME composite is shown in Fig. 1(f). The three-dimensional view of the *ME flux gate* sensor and its forced vibration mode (at non-resonant frequency) under H_{AC} excitation are presented in Fig. 3(a-i) and (a-ii), respectively. We then verified the theoretical analysis concerning the proposed MEFGS experimentally. Figure 3(b) shows differential signal output ΔV_{ME} (at non-resonant frequency $f = 48.5$ kHz) under different magnetic anomaly H_{DC}, which was observed directly from a mixed digital signal oscilloscope (Keysight 4024 A). It can be clearly seen that ΔV_{ME} is near zero when $H_{DC} = 0\ \mu T$. Once a *DC* magnetic field of 2 or 4 μT appears, a dramatic differential ME signal (*first harmonic*) is produced from the *ME flux gate* sensor. The measured results agree well with those as expected in Fig. 2(d).

Figure 3(c) shows the measured frequency responses of ME electric field coefficient α_{ME} of the MEFGS. The ME coupling coefficient α_{ME} for each half of the shuttle shape ME sensor are 22.6 and 22.2 $V/cmOe$ at non-resonance; while at resonance frequency of 20.02 kHz, it dramatically increases to 2918 and 2894 V/cm_*Oe, respectively. It can be seen from the measured frequency spectrum characteristics as presented in Fig. 3(d) that the two halves of the MEFGS structure exhibit quite similar ME performance, proving that they are wonderful symmetric. The sum output of the two halves even reaches to 5700 V/cmOe, which is close to the best result reported in one dimensional (1-1) ME composite[19].

It is widely known that ME composite materials exhibit the strong magnetoelectric coupling at resonance, therefore, a high magnetic field sensitivity at resonant frequency should be expected. *Chu et al*. develpoed a one-dimensional [011]-oriented PMN-PT/Metgals (1-1) composite, which had a limit *AC* magnetic field sensitivity as low as 1.35×10^{-13} Tesla at resonant frequency[19]. *Gao et al*. reported a (2-1) Metglas/PMN–PT laminate sensors showing a *DC* magnetic field sensitivity as high as (i) 5 nT at 1 kHz and (ii) 1 nT near the resonant frequency in a shield chamber[25].

High sensitivity to weak DC magnetic field. In this work, we investigate the *DC* magnetic field responses of the MEFGS in the both cases of resonance and non-resonance frequencies. Measurements of magnetic field sensitivity was carried out in a shielded chamber with a lock-in amplifier. We found that under exciting of a closed-loop H_{AC} with the frequency of $f = 10.5$ kHz, the MEFGS exhibits a strong resonant response at $f_r = 21$ kHz, because of the frequency-double effect. We then observed H_{DC} response at $f = 10.5$ kHz due to "frequency-doubling" to "same-frequency" effect. Figure 4 shows the measured ME differential voltage response to a weak and step-varying H_{DC}. As shown in Fig. 4(a), a step-varying δH_{DC} of 4 nT could be distinguished clearly, and the ME differential signal was also able to return to the initial level. However, when further decreasing δH_{DC} to be 2 nT, we found the noise level becomes non-ignorable, as shown in Fig. 4(b). Apparently, noise level at resonance is a main obstacle to the detection of an extremely weak *DC* magnetic field. In order to improve *DC* magentic field sensitivity, it seems that H_{AC} exciting at resonant frequency is unnecessary, because it could increase the

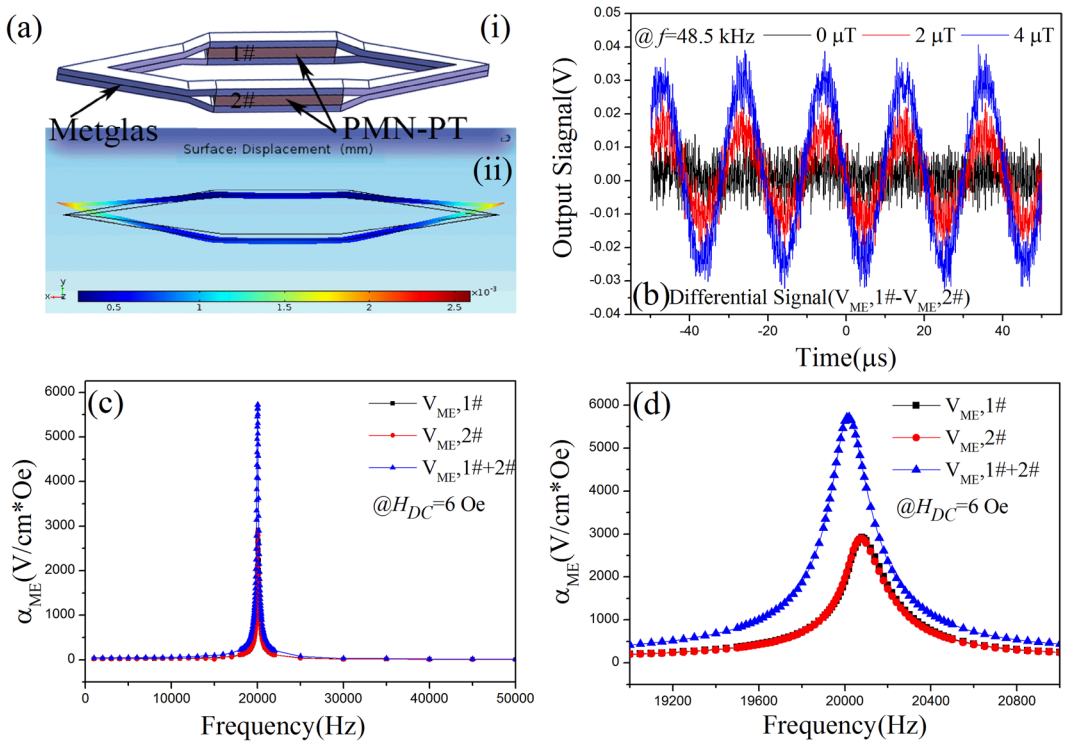

Figure 3. The experimental verification concerning the working principle and the ME performance for our proposed ME Gate sensor. (**a-i**) Three-dimensional view of the ME flu gate sensor made of a laser-treated Metglas magnetic core (shuttle shape) and one pair of [011]-oriented PMN-PT single crystal fibers (as labeled as 1# and 2#) embedded in the magnetic core; (**a-ii**) A schematic view of the forced vibration mode at non-resonant frequency. (**b**) The differential signal output of the MEFGS in response to varying DC magnetic field at 0 μT, 2 μT, 4 μT, respectively; The frequency response of ME coupling coefficient $\alpha_{ME,1\#}$, $\alpha_{ME,2\#}$ and $\alpha_{ME,1\#+2\#}$ of the MEFGS in frequency range from 1 to 50 kHz (**c**), and 19 to 21 kHz (**d**). Here, $\alpha_{ME,1\#+2\#}$ is the sum ME signal output of two halves of the MEFGS when the two terminals are connected in series.

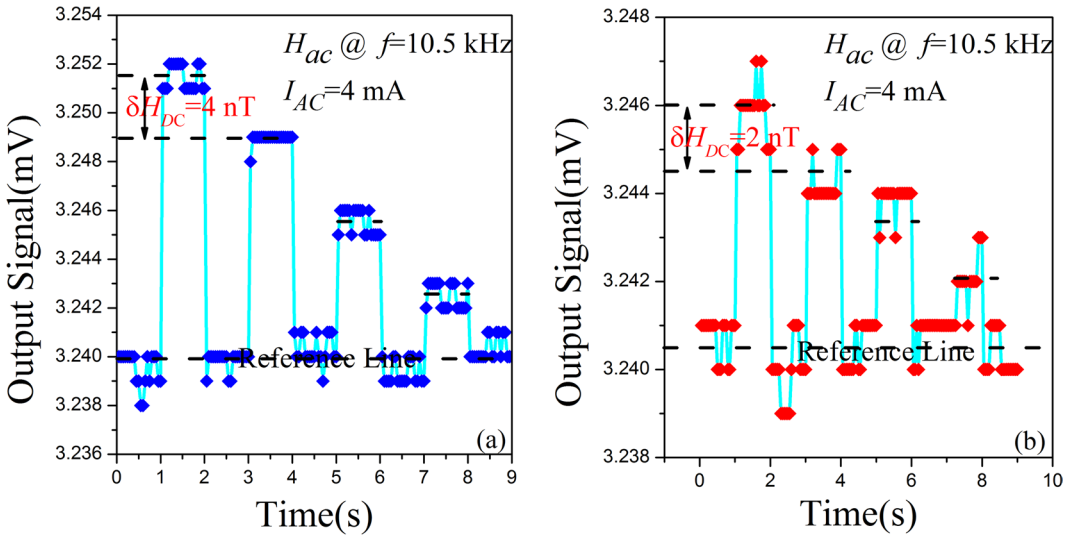

Figure 4. ME voltage output signal of the MEFGS in response to a weak step-varying DC magnetic field at the first-order longitudinal vibration mode (fr1 = 10.5 kHz). (**a**) In response to a step of 4 nT. (**b**) In response to a step of 2 nT.

undesired noise greatly (althogh it also improves ME coupling greatly). In our case, lowering noise of MEFGS and obtaining a stable vibration condition are eseential for sensing an extremely low *DC* magneitc field.

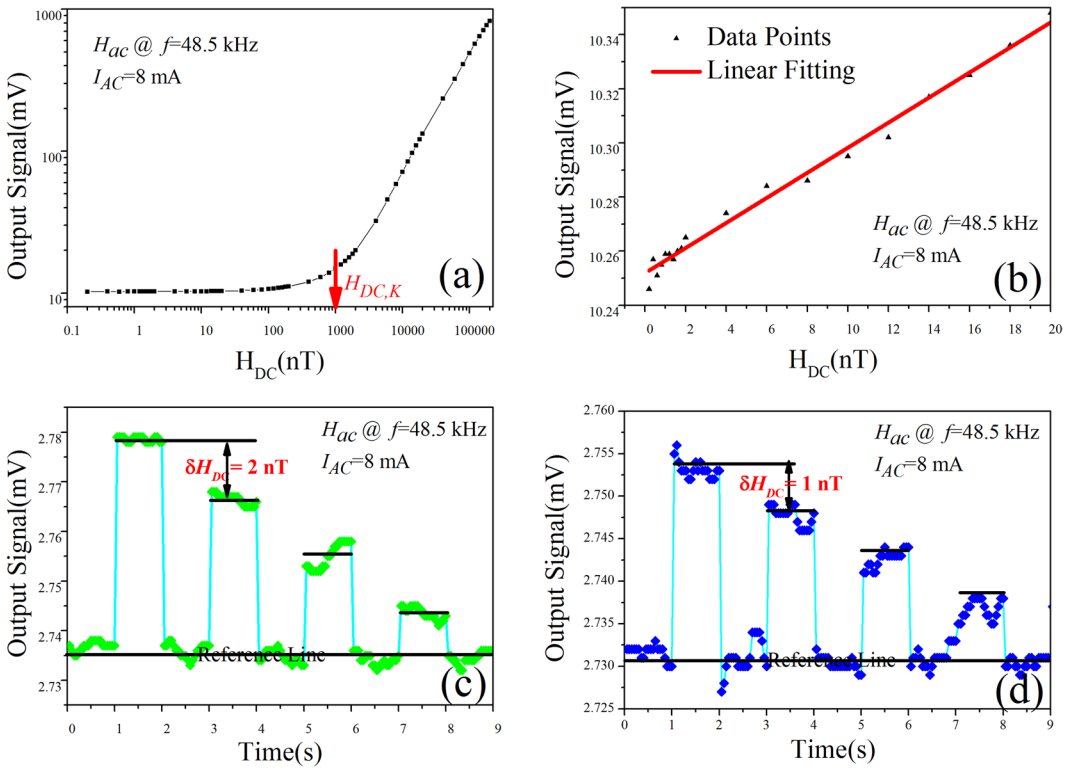

Figure 5. Charaterization for weak DC magneitic field measured at non-resonat frequency. (**a**) The magnetic field sensitivity in terms of DC magnetic field varying from 0.2 to 2 $*$ 10^5 nano Tesla at non-resonant frequency of 48.5 kHz. (**b**) The zoomed area of (**a**) with DC magnetic field starting from 0.2 to 20 nano Tesla. ME voltage output signal in response to an extremely weak step-varying DC magnetic field of 2 nT (**c**)and 1 nT (**d**) at f = 48.5 kHz, which is far deviate from the resonant frequency of the MEFGS.

Finally, we investigate the *DC* magnetic field responses of the MEFGS in non-resonance frequency range, including its limit of detection (LOD) of *DC* magnetic field. We chose a much higher working frequency around 48.5 kHz for exciting *AC* magnetic field in the closed-loop magnetic core of MEFGS, which is deviated far from the resonant state of the MEFGS. Since it is a non-resonance forced vibration mode, we accordingly increase the *AC* current for produing a relatively higher H_{AC}. Figure 5(a) shows the measured differential ME voltage output signal in response to an applied H_{DC} varying from 0.2 to 200000 nT. Apparently, there is a *knee* $H_{DC,K}$ or threshold about 1000 nT. When H_{DC} is higher than $H_{DC,K}$, the MEFGS exhibits a strong linear-response to the applied H_{DC} with a large slope. While H_{DC} is lower than $H_{DC,K}$, the MEFGS shows a weak linear-responses to H_{DC} with a small slope, which may be attributed to interface effect of ferromagnetic and ferroelectric two phase, including interface strain transfer loss and interface voltage drop at bonding layer (like a capacitor)[43]. Figure 5(b) shows the zoomed area where *DC* magnetic field is limited in a small range, starting from 0.2 to 20 nT. It is clearly seen that output signal exhibits a linear relationship with H_{DC} starting from 1 nT. Measurement values then become scattering when H_{DC} is less than 1 nT. However, the LOD value of H_{DC} can be clearly seen to be 2 nT and 1 nT, respectivelly, as presented in Fig. 5(c), and Fig. 5(d), revealing a superhigh *DC* magnetic field sensitivity of the MEFGS. It should be noted here that the relative changes of the ME voltage output signal in response to 1 nT is only 0.2%, but it is still nearly 4 to 5 times higher in comparison with previously measurements on 1 nT *DC* magnetic field detection[25]. This result is significant, which shows that a *ME flux gate* sensor under exciting of non-resonant high frequency H_{AC} may have higher *DC* magnetic field sensitivity due to lower vibration noise, which is apparently different from the previous claims in conventional ME sensors[25,44]. In addition, there is no need to apply a bias field for achieving a LOD value of 1 nT in present work.

Discussion

To further improve the MEFGS, following jobs are necessary: (i) improving symmertry about two halves of the MEFGS structure for lowering noise; (ii) decreasing interface effect of ferromagnetic and ferroelectric two phases for lowering *knee* $H_{DC,K}$; and (iii) optimizing *ME* working mode for obtaining a more stable performance. (iv) seeking piezoelectric materials with lower dielectric loss and piezomagetic materials with higher piezomagetic property. Proposed MFFGS shows high *DC* field detection sentivity that has significant potential toward pratical application in magnetic navigation systems and medical diagnosis.

In summary, a *DC* magnetic field sensor working on magnetoelectric coupling effect and *flux gate* principle (named as *MEFGS*) is proposed for the first time; its principle in comparison with the conventional *flux gate* sensor is analyzed theoretically and then confirmed experimentally. MEFGS is composed of a shuttle-shaped, laser-treated, and multilayered amorphous FeBSi alloy (Metglas) magnetic core and one pair of embedded

[011]-oriented $Pb(Mg,Nb)O_3$-$PbTiO_3$ (PMN-PT) single crystal fibers. The fabricated MEFGS exhibits the strong ME coupling: non-resonance ME coefficients of two halves in the shuttle-shape structure are 22.6 and 22.28 V/cm Oe, respectively; while at resonance, they are dramatically increased to 2918 and 2894 V/cm Oe, respectively. These results also show well symmetry of the shuttle shape structure, which is important to a flux gate magnetic sensor due to its differential working mode. It was further found that the MEFGS has a wide response to *DC* magnetic field ranging from 0.2 to 200000 nT, accompanying a *knee* $H_{DC,K}$ or threshold phenomenon at $H_{DC} = 1000$ nT possibly due to interface effect. The repeatable, absolute limit of detection (LOD) of *DC* magnetic field is found to be 1 nT at non-resonant frequency and at room temperature without bias magnetic field. The relative change of output signal of the MEFGS at 1 nT is 4 to 5 times higher in comparison with the previous reports. Proposed MEFGS can be viewed as a potential alternative ultra-sensitive *DC* magnetic field sensor, like *flux gate* sensor in particular, which shows significant availability toward practical application in magnetic navigations and magnetic based medical diagnosis because of very low power consumption and fine structure.

Methods

ME performance characterization. the ME coefficient was measured at room temperature using a home-made setup. A purchased Helmholtz coil and a *DC* current supply (IT6932A, ITECH, USA) were used to produce a direct current (*DC*) magnetic field bias (0–6 Oe). And a home-made Helmholtz coil carrying a standard *AC* current (6221, Keithley, USA) was used to generated an *AC* magnetic field. The induced voltages from two piezoelectric sensing elements (PMN-PT single crystal,1# and 2#) were measured with a lock-in amplifier (SR850, Stanford Research, USA), the time constant (integration time) and the bandwidth of which were set at 100ms and 1.2 Hz, respectively.

DC magnetic field measurement. As presented in Fig. 1(d), the two halves of the magnetic core are exposed to a common applied *DC* filed H_{DC} (a small quantity) and to the *AC* excitation field H_1 and H_2, respectively. Since the two terminals were winded with an opposite direction, H_1 is completely reverse to H_2. Here the *DC* magnetic field was excited with a purchased solenoid coil carrying a standard *DC* current (6221, Keithley, USA) and the AC magnetic field was generated through home-made coils (the number of turns is 200 for each half as shown in Fig. 1(d)) excited by a Function/Arbitrary Waveform Generator (Agilent 33522 A). In addition, the induced differential voltage variations from two piezoelectric sensing elements (PMN-PT single crystal, 1# and 2#) were measured with a lock-in amplifier (SR850, Stanford Research, USA).

Data availability. The datasets generated analysed during the current study are available from the corresponding author on reasonable request.

References

1. Hu, J., Chen, L. & Nan, C. W. Multiferroic heterostructures integrating ferroelectric and magnetic materials. *Adv. Mater.* **28**, 15 (2016).
2. Eom, C. & McKinstry, S. Thin-film piezoelectric MEMS. *MRS Bull.* **37**, 1007 (2012).
3. Scott, J. Applications of modern ferroelectrics. *Science* **315**, 954 (2007).
4. Wang, K., Alzate, J. & Amiri, P. Low-power non-volatile spintronic memory: STT-RAM and beyond. *J. Phys. D: Appl. Phys.* **46**, 047003 (2013).
5. Nan, C. W., Bichurin, M. I., Dong, S. X., Viehland, D. & Srinivasan, G. Multiferroic magnetoelectric composites: historical perspective, status, and future directions. *J. Appl. Phys.* **103**, 031101 (2008).
6. Annapureddy, V. *et al*. Low-Loss Piezoelectric Single-Crystal Fibers for Enhanced Magnetic Energy Harvesting with Magnetoelectric Composite. *Adv. Energy Mater.* **6**, 1601244 (2016).
7. Wang, Y. J., Li, J. F. & Viehland, D. magnetoelectrics for magnetic sensor applications: status, challenges and perspectives. *Mater. Today*. doi:10.1016/j.mattod.2014.05.004 (2014).
8. Zhai, J. Y., Xing, Z. P., Dong, S. X., Li, J. F. & Viehland, D. Magnetoelectric laminate composites: an overview. *J. Am. Ceram. Soc.* **91**, 51 (2008).
9. Palneedi, H., Annapureddy, V., Priya, S. & Ryu, J. Status and perspectives of multiferroic magnetoelectric composite materials and applications. *Actuators* **5**, 9 (2016).
10. Ma, J., Hu, J. M., Li, Z. & Nan, C. W. Recent progress in multiferroic magnetoelectric composites: from bulk to thin films. *Adv. Mater.* **23**, 1062 (2011).
11. Ramesh, R. & Spaldin, N. A. Multiferroics: progress and prospects in thin films. *Nat. Mater.* **6**, 21 (2007).
12. Ma, J., Shi, Z. & Nan, C. W. Magnetoelectric Properties of Composites of Single $Pb(Zr,Ti)O_3$ Rods and Terfenol-D/Epoxy with a Single-Period of 1-3-Type Structure. *Adv. Mater.* **19**, 2571 (2007).
13. Dong, S. X., Li, J. F. & Viehland, D. A longitudinal-longitudinal mode TERFENOL-D/Pb $(Mg1/3Nb2/3)O_3$-$PbTiO_3$ laminate composite. *Appl. Phys. Lett.* **85**, 5305 (2004).
14. Zhai, J. Y., Dong, S. X., Xing, Z. P., Li, J. F. & Viehland, D. Giant magnetoelectric effect in Metglas/polyvinylidene-fluoride laminates. *Appl. Phys. Lett.* **89**, 083507 (2006).
15. Jin, J. Z. *et al*. Multiferroic polymer composites with greatly enhanced magnetoelectric effect under a low magnetic bias. *Adv. Mater.* **23**, 3853 (2011).
16. Dong, S. X., Zhai, J. Y., Li, J. F. & Viehland, D. Near-ideal magnetoelectricity in high-permeability magnetostrictive/piezofiber laminates with a (2-1) connectivity. *Appl. Phys. Lett.* **89**, 252904 (2006).
17. Dong, S. X., Zhai, J. Y., Xing, Z. P., Li, J. F. & Viehland, D. Giant magnetoelectric effect (under a dc magnetic bias of 2 Oe) in laminate composites of FeBSiC alloy ribbons and $Pb(Zn1/3, Nb2/3)O_3$-7% $PbTiO_3$ fibers. *Appl. Phys. Lett.* **91**, 022915 (2007).
18. Gao, J. Q., Shen, L. G., Wang, Y. J., Gray, D. J. F. & Viehland, D. Enhanced sensitivity to direct current magnetic field changes in Metglas/$Pb(Mg1/3Nb2/3)O_3$-$PbTiO_3$ laminates. *J. Appl. Phys.* **109**, 074507 (2011).
19. Chu, Z. Q. *et al*. Enhanced Resonance Magnetoelectric Coupling in (1-1) Connectivity Composites. *Adv. Mater.* **29**, 1606022 (2017).
20. Kirchhof, C. *et al*. Giant magnetoelectric effect in vacuum. *Appl. Phys. Lett.* **102**, 232905 (2013).
21. Yarar, E. *et al*. Inverse bilayer magnetoelectric thin film sensor. *Appl. Phys. Lett.* **109**, 022901 (2016).
22. Liu, Y. *et al*. Frequency conversion in magnetoelectric composites for quasi-static magnetic field detection. *Appl. Phys. Lett.* **103**, 212902 (2013).
23. Jahns, R., Greve, H., Woltermann, E., Quandt, E. & Knöchel, R. Sensitivity enhancement of magnetoelectric sensors through frequency-conversion. *Sensors and Actuators A* **183**, 16 (2012).

24. Nan, T. X., Hui, Y., Rinaldi, M. & Sun, N. X. Self-biased 215 MHz magnetoelectric NEMS resonator for ultra-sensitive DC magnetic field detectt. *Sci. Rep.* **3**, 1985, doi:10.1038/srep01985 (2013).
25. Gao, J. *et al*. Enhanced sensitivity to direct current magnetic field changes in Metglas/Pb (Mg1/3Nb2/3) O3–PbTiO3 laminates. *J. Appl. Phys.* **109**, 074507 (2011).
26. Mahdi, A., Panina, L. & Mapps, D. Some new horizons in magnetic sensing: high-Tc SQUIDs, GMR and GMI materials. *Sens. Actuators A* **105**, 271 (2003).
27. Li, P. *et al*. Electric Field Manipulation of Magnetization Rotation and Tunneling Magnetoresistance of Magnetic Tunnel Junctions at Room Temperature. *Adv. Mater.* **26**, 4320 (2014).
28. Karnaushenko, D. *et al*. High-Performance Magnetic Sensorics for Printable and Flexible Electronics. *Adv. Mater.* **27**, 880 (2015).
29. Karnaushenko, D. *et al*. Self-Assembled On-Chip-Integrated Giant Magneto-Impedance Sensorics. *Adv. Mater.* **27**, 6582 (2015).
30. Wang, Z. L. *et al*. Highly Sensitive Flexible Magnetic Sensor Based on Anisotropic Magnetoresistance Effect. *Adv. Mater.* **28**, 9370 (2016).
31. Ripka, P. Advances in fluxgate sensors. *Sensors and Actuators A* **106**, 8–14 (2003).
32. Quesada, G., Lumbreras, M., Delagdo, R. & Roca, A. Class H Power Amplifier for Power Saving in Fluxgate Current Transducers. *IEEE Sonseors J.* **16**, 2322 (2016).
33. Lu, C., Huang, J., Chiu, P., Chiu, S. & Jeng, J. High-sensitivity low-noise miniature fluxgate magnetometers using a flip chip conceptual design. *Sensors* **14**, 13815 (2014).
34. Primdahl, F. The Fluxgate Mechanism, Part I: The Gating Curves of Parallel and Orthogonal Fluxgates. *IEEE Trans. Magn.* **MAG-6**, 376 (1970).
35. Ripka, P. Race-track fluxgate with adjustable feedthrough. *Sensors and Actuators* **85**, 227 (2000).
36. Koch, R., Deak, J. & Grinstein, G. Fundamental limits to magnetic-field sensitivity of flux-gate magnetic-field sensors. *Appl. Phys. Lett.* **75**, 3862 (1999).
37. Yang, X. *et al*. Design and realization of a novel compact fluxgate current sensor. *IEEE Trans. Magn.* **51**, 4002804 (2015).
38. Ma, J., Li, Z., Lin, Y. & Nan, C. W. A novel frequency multiplier based on magnetoelectric laminate. *Journal of Magnetism and Magnetic Materials* **323**, 101–103 (2011).
39. Zhang, W. H., Yin, G., Cao, J. W., Bai, J. M. & Wei, F. L. Frequency multiplying behavior in a magnetoelectric unimorph. *Appl. Phys. Lett.* **100**, 032903 (2012).
40. Xu, H., Pei, Y. & Fang, D. The frequency dependence of harmonic hysteresis effect in magnetoelectric laminated composites. *Compos. Struct.* **147**, 33 (2016).
41. Shi, Y. & Gao, Y. Theoretical study on nonlinear magnetoelectric effect and harmonic distortion behavior in laminated composite. *Journal of Alloys and Compounds* **646**, 351–359 (2015).
42. Burdin, D. *et al*. DC magnetic field sensing based on the nonlinear magnetoelectric effect in magnetic heterostructures. *J. Phys. D: Appl. Phys.* **49**, 375002 (2016).
43. Zhang, B. N., Zhang, J. Q., & Huang, S. L. Deformation transfer in smart structures with integrated piezoceramic sensors. *Journal of Chongqing University* (2000)
44. Dong, S., Zhai, J., Li, J. & Viehland, D. Small dc magnetic field response of magnetoelectric laminate composites. *Appl. Phys. Lett.* **88**, 082907 (2006).

Acknowledgements

This work was supported by the National Natural Science Foundation of China (Grant Nos 51132001, 51072003); Beijing Municipal Science and Technology Projects (Grant Nos Z131100003213020, Z151100003715003).

Author Contributions

Z. Chu performned most the experiments and data analysis with help from H. Shi, W. Shi and M. PourhosseiniAsl; J. Wu, X. Gao and X. Yuan performed the materials fabrication and analysis about the interfacial structure of our proposed magnetoelectric flux gate sensor, S. Dong dircted and advised this research. S. Dong and Z. Chu wrote the manuscript with the input from all the authors. All authors reviewed the manuscript.

Additional Information

Competing Interests: The authors declare that they have no competing interests.

Publisher's note: Springer Nature remains neutral with regard to jurisdictional claims in published maps and institutional affiliations.